Highly Permeable Mixed Matrix Membranes of Thermally Rearranged Polymers and Porous Polymer Networks for Gas Separations

Carla Aguilar-Lugo[1,2] Won Hee Lee[3], Jesús A. Miguel[4], José G. de la Campa[1], Pedro Prádanos[5], Joon Yong Bae[3], Young Moo Lee[3,], Cristina Álvarez[1,5,*], Ángel E. Lozano[1,4,5,*]*

1 Institute of Polymer Science and Technology, ICTP-CSIC, Juan de la Cierva 3, 28006 Madrid, Spain.

2. Instituto de Investigaciones en Materiales. Universidad Nacional Autonoma de Mexico, IIM-UNAM, Circuito Exterior S/N, Circuito de la Investigación Científica, Ciudad Universitaria, 04510 Cd. Mx., Mexico

3 Department of Energy Engineering, College of Engineering, Hanyang University, 04763 Seoul, Republic of Korea.

4 IU CINQUIMA, University of Valladolid, 47071 Valladolid, Spain.

5 SMAP UVa-CSIC Research Unit, University of Valladolid, 47071 Valladolid, Spain.

KEYWORDS: Thermal rearrangement; Gas separation; Microporous polymer network; Mixed matrix membranes; Thermal resistance

ABSTRACT

Mixed matrix membranes (MMMs) have been obtained by blending an aromatic *ortho*-hydroxypolyimide (PIOH) or an *ortho*-acetylpolyimide (PIOAc) with different loading amounts (15 and 30 wt%) of a microporous polymer network (PPN), which was obtained from the reaction of triptycene and isatin. The excellent thermal resistance of the PPN (above 500 °C) allowed it to be used as a filler to successfully prepare thermally rearranged polybenzoxazole (TR-PBO)-MMMs obtained from the thermal treatment of the above MMMs. Moreover, PPN showed relatively good compatibility with the polyimide matrix, which improved the TR-PBO formation. The gas separation performances of these MMM_S before and after the thermal process were studied for five representative gases (He, O_2, N_2, CO_2 and CH_4). For the MMMs derived from *ortho*-

functional polyimides, the gas permeability considerably increased for all the gases, whereas the selectivity for gas pairs, such as CO_2/N_2 and CO_2/CH_4, remained similar. Thus, the selectivity-permeability performance of PIOH- and PIOAc-MMMs containing 30 wt% of PPN (PIOH30 and PIOAc30) surpassed the 1991 Robeson limit for the CO_2/CH_4 gas pair. In the case of TR-PBO-MMMs (TROH and TROAc-MMMs), the thermal rearrangement process led to an increase in the gas permeability, showing values much better than those observed for the TR-PBO material employed as a MMM matrix. The selectivity values were a little bit lower than the pristine TR-PBO membranes. The CO_2 permeability of TROAc30 was 1036 barrer with a CO_2/CH_4 selectivity of 28, surpassing the 2008 Robeson limit.

INTRODUCTION

Polymer membranes can be used to separate complex mixtures of gases.[1–5] However, classical approaches are not able to meet the needs of industry to obtain materials having large gas separation productivity in harsh conditions.[6,7] In this context, thermal and chemical resistant polymeric materials are extensively sought for use in industry.[3,8,9]

Thermally rearranged (TR) polymer membranes have been of interest due to their outstanding gas permeability.[9–15] TR polymers are materials where solid-state molecular rearrangements from a rigid structure to another more rigid and stable structure are carried out by a thermal treatment at relatively high temperature.[9,12,16–19] Due to this thermal conversion, materials with very high permeability and good selectivity have been obtained. In particular, some sets of new gas separation membranes based on polyimides (PIs) having *ortho*-hydroxy groups, capable of yielding thermally rearranged polybenzoxazoles (TR-PBOs), have been developed.[4,20–22] These membranes are extremely efficient to separate CO_2 from other gases. In fact, they are so efficient that their properties can be compared with those of the carbon molecular sieves, but with much better mechanical properties.[23–27] Further, due to the formation of a very rigid polymer structure during the thermal treatment, these TR-PBO membranes show low physical aging and acceptable resistance to plasticization.[28]

The preparation of mixed matrix membranes (MMMs), which combine a linear polymer showing high gas permeability with metal organic frameworks (MOF and ZIFs),[29–33] porous organic frameworks (PAFs),[34,35] or porous polymer networks (PPNs),[36] has provided novel materials with excellent gas permeability and selectivity. However,

the use of PPNs as fillers in MMMs where the polyimide matrix is going to undergo an additional thermal rearrangement (TR) process is more cumbersome due to the high temperature at which the TR takes place (above 400 °C).[37–39] Thus, the PPNs should have degradation temperatures near 500 ºC to preserve their macromolecular structure during the thermal rearrangement.[40]

In this context, our group has developed a feasible and low-cost synthetic protocol to prepare high-thermal and chemical stable PPNs by reaction of rigid triaromatic compounds (having a required symmetry) with ketones that have electron-withdrawing groups.[41] Some of these PPNs exhibited high chemical resistance and exceptional thermal stability (degradation onset above 450 °C). Moreover, they showed highly microporous structures, with Brunauer-Emmet-Teller (BET) surface areas of up to of 800 $m^2 g^{-1}$ and CO_2 uptakes of up to 207 mg g^{-1} (105 cm^3(STP) g^{-1}) at 273 K and 1 bar.

Recently, we have employed one of these high-thermal stable PPNs, specifically one derived from triptycene and isatin, as a filler to prepare MMMs using three polyimides matrices: a commercial one, Matrimid, and two others synthesized by us, 6FDA-6FpDA and 6FDA-TMPD, which are commonly employed in gas separation studies.[42–46] Homogeneous MMMs with excellent mechanical properties and better gas separation

performances for CO_2/CH_4 and CO_2/N_2 than those of the pristine polyimide membranes were obtained.[47]

The present study extended the use of the triptycene-isatin PPN to prepare TR-PBO-MMMs employing two previously reported TR-able polyimides that were derived from 3,3'-dihydroxybenzidine (HAB) and 2,2'-bis-(3,4-dicarboxyphenyl)hexafluoropropane dianhydride (6FDA): *ortho*-hydroxy and *ortho*-acetyl polyimides, referred to here as PIOH and PIOAc, respectively.[12] Dynamic and isothermal thermogravimetric analysis measurements were carried out to optimize the TR-conversion protocol in the presence of the PPN. The validity of using this high-thermal stable filler to improve the performances of the TR-PBO-MMMs was evaluated by comparing the gas separation and mechanical properties of MMMs before (PI-MMMs) and after thermal rearrangement (TR-PBO-MMMs). The aim of this work is to show how the high microporosity and the excellent thermal stability derived from the PPNs impart improved CO_2 permeability to TR-PBO-MMMs, while retaining sufficient mechanical properties to be tested for gas separation applications.

2. EXPERIMENTAL SECTION

2.1. Materials

3,3'-Dihydroxybenzidine (HAB) and 2,2'-bis-(3,4-dicarboxyphenyl)hexafluoropropane dianhydride (6FDA) were supplied by TCI Europe. The HAB diamine was dried at 120 °C for 5 h under vacuum, and the 6FDA dianhydride was sublimated at 220 °C prior to use. Triptycene (98% of purity) was purchased from abcr GmbH, isatin (1H-indole-2,3-dione, 99% of purity) from Sigma-Aldrich, and they were dried at 80 °C under vacuum before use. Chlorotrimethylsilane (CTMS), pyridine (Py), 4-dimethylaminopyridine (DMAP), *o*-xylene, acetic anhydride, N,N-dimethylacetamide (DMAc), tetrahydrofuran (THF) and anhydrous N-methyl -2pyrrolidinone (NMP) were supplied by Sigma-Aldrich and used as received. Trifluoromethanesulfonic acid (TFSA, 99.5% of purity) was obtained from Apollo Scientific.

2.2. Synthesis of polyimides

The *ortho*-hydroxypolyimide (PIOH) and *ortho*-acetylpolyimide (PIOAc) were synthesized from the HAB diamine and the 6FDA dianhydride following the *in situ* silylation methodology[48,49] and the routes reported in a previous work.[12,16] The synthesis consisted of the preparation of the *ortho*-hydroxy poly(amic acid) (HPAA) followed by

its subsequent conversion to PIOH via azeotropic imidization and to PIOAc via chemical imidization.

2.2.1. *Synthesis of ortho-hydroxypolyimide*

First, 10.0 mmol of HAB and 10 mL of NMP were added to a round bottomed three-neck flask equipped with mechanical stirrer and nitrogen inlet and outlet and were stirred at room temperature under a dry nitrogen atmosphere until HAB was dissolved in NMP. It is appropriate to point out that the mechanical stirring and the nitrogen atmosphere were maintained during all the steps of the reaction unless indicated. The solution was cooled to 0 °C, the required amounts of CTMS (1 mol/mol reactive group) and Py (1mol/mol reactive group) were added to the solution, and the temperature was raised to room temperature and maintained for 15 min to ensure the formation of the silylated diamine.[48,49] Next, the solution was cooled once again to 0 °C, and 10.0 mmol of 6FDA were added followed by DMAP (0.1 mol/mol Py) and 10 mL of NMP. The reaction mixture was then stirred for 15 min at 0 °C and left overnight at room temperature for the complete formation of the HPAA. Afterwards, 20 mL of *o*-xylene were added to the HPAA solution, and the reaction mixture was heated at 180 °C for 6 h. The water released during the imidization step was separated out as a xylene azeotrope, along with silanol

and other siloxane by-products derived from the use of silylating agent. Finally, the additional *o*-xylene was stripped out from the polyimide solution, which was then cooled to room temperature and poured into distilled water. The precipitated polymer was washed several times with water, then a mixture of water/ethanol (1/1), then pure ethanol. Finally, it was dried at 150 °C for 12 h under vacuum. **PIOH**: η_{inh}= 0.70 dL/g. ^{1}H-NMR.[16]

2.2.2. *Synthesis of ortho-acetylpolyimide*

The HPAA solution was prepared in the same manner as described above, but DMAc was used as a solvent instead of NMP. A mixture of acetic anhydride (80 mmol, 4 mol/mol reactive group) and Py (80 mmol, 4 mol/mol reactive group) was added to the HPAA solution, which was stirred for 6 h at room temperature and 1 h more at 60 °C to promote the cycloimidization. The polymer solution was cooled to room temperature and poured into distilled water. The polymer was washed several times with water, then it was washed with a mixture water/ethanol (1/1), and finally dried in a vacuum oven at 150 °C overnight. **PIOAc:** η_{inh}= 0.52 dL/g. ^{1}H-NMR.[16]

2.3. Synthesis of the triptycene-isatin PPN

The triptycene-isatin PPN was obtained in quantitative yield by reacting triptycene and isatin in a superacidic media according to the procedure previously reported by our

group.[41] Thus, 23.0 mmol of triptycene, 34.5 mmol of isatin and 25 mL of chloroform were added to a three-necked Schlenk flask, equipped with a mechanical stirrer and gas inlet and outlet. The mixture was stirred at room temperature under a nitrogen blanket, then cooled to 0 °C. Then, 50 mL of TFSA were slowly added to the mixture with an addition funnel for 30 min. Next, the reaction mixture was allowed to warm to room temperature and stirred for 5 days. The solid was poured into a water/ethanol mixture (3/1), filtered, consecutively washed with hot water, acetone, chloroform and acetone and, finally, dried in a vacuum oven at 150 °C for 12 h. CP/MAS ^{13}C NMR (100 MHz, solid state) δ ppm: 180, 145, 124, 110, 62, 55.[41]

2.4. Membrane fabrication

The MMMs with targeted PPN loading (15 and 30 wt.% of total solid weight: PPN + polymer) were prepared following the methodology reported earlier by our group.[47] First, the required amount of PPN was dispersed in THF (10 mL) by stirring for 24 h at room temperature, followed by sonication for 20 min with a 130 W ultrasonic probe (Vibra Cell™ 75186) operating at 25% maximum amplitude. The procedure consisted of 40 cycles of 20 s ultrasonic exposures and 10 s cool-down so that the particles could be entirely dispersed. Next, about half the volume of the polymer solution (500 mg of polymer in 5 mL of THF) was added to the stirring suspension of the filler, which was subsequently sonicated in the same previous conditions for 10 min (20 cycles) before adding the rest of the polymer solution. After stirring for a further 30 min, the final

suspension was poured into a glass ring placed on a leveled glass plate, covered with a watch-glass. It was raised slightly and left at room temperature overnight to remove most of the solvent. The films were peeled off from the glass plate and subjected to the following thermal treatment under vacuum conditions: 100 °C for 1 h, 150 °C for 1 h, 180 °C for 1 h, 250 °C for 1h min, and they then were allowed to cool slowly. The film thickness range was 40-50 μm. MMMs obtained from PIOH and PIOAc were designated as PIOHX and PIOAcX, where X is the weight percent of PPN in the final suspension.

For comparative purposes, neat polyimide films were cast following the protocol described above. The casting of polyimide was done from a filtered 10% polymer solution in THF.

Note that additional MMMs were similarly prepared from PPN solid previously subjected to a CO_2 plasma treatment for 30 min to test the possible effect of this treatment on the compatibility of the filler and polymer matrix, and consequently on the gas separation properties. The MMMs prepared using the plasma-treated PPN were designated adding the suffix PL to the designation of the MMMs, e.g., PIOAcX_PL and TROAcX_PL. Details of the plasma treatment are given in the Section 2.6.

2.5. Thermal rearrangement protocol

Circle membrane coupons of PIOH, PIOAc, PIOHX and PIOAcX were cut into 3 cm^2 pieces, sandwiched between ceramic plates to avoid film rolling at elevated temperatures and placed in a quartz tube furnace in a high-purity nitrogen atmosphere (0.3 L min^{-1}). Samples were heated to 275 °C at a heating rate of 20 °C min^{-1}, then to 300 °C at 5 °C min^{-1} and held for 1 h for complete solvent removal. Then, the membranes were further heated to a particular rearrangement temperature (350, 400, 425 and 450 °C) with a heating rate of 5 °C min^{-1} and held for the desired time (0.5 or 1 h). Afterwards, the furnace was cooled to room temperature at a rate no greater than 10 °C min^{-1}. Thermally rearranged membranes were designated as TROHX-T/t and TROAcX-T/t, where X is the weight percent of PPN, T the final rearrangement temperature, and t is the dwell time at T.

2.6. Plasma modification

The CO_2-plasma surface treatment of the PPN was carried out on 2.0 g of the porous polymer solid using a Harrick PDC-002 plasma-cleaner device where the sample was positioned in the medium of the quartz plasma cylinder. The operating radio-frequency power was kept at 10 W (medium position), and the chamber pressure was kept at 200-250 Torr with a CO_2 flow of 25 mL min^{-1}. The time of the treatment was 30 min.

2.7. Characterization

Attenuated total reflection-Fourier transform infrared (ATR-FTIR) spectra were registered on a Perkin Elmer Spectrum RX-I FTIR spectrometer equipped with an ATR accessory. Inherent viscosities of polymers were measured at 30 °C with an Ubbelohde viscometer using NMP as a solvent at 0.5 g dL^{-1}. Thermogravimetric analysis (TGA) was performed on a TA Q-500 thermobalance under a nitrogen atmosphere (60 mL min^{-1}). Dynamic TGA was conducted at 10 °C min^{-1} from 30 to 850 °C. Isothermal TGA was conducted using the following thermal protocol: the sample was heated at 300 °C and held at this temperature for 1h and then heated at a rearrangement temperature (350, 400, 425 and 450) at 5 °C min^{-1} and held for 1 h. Wide-angle-X-ray scattering (WAXS) patterns were recorded in the reflection mode at room temperature using a Bruker D8 Advance diffractometer provided with a Goebel Mirror and a PSD Vantec detector. CuKα (wavelength λ = 1.54 Å) radiation was used. A step-scanning mode was employed for the detector, with a 2θ step of 0.024˚ and 0.5 s per step. Scanning electron microscopy (SEM) images were taken with a QUANTA 200 FEG ESEM on Au-metallized samples operating at an acceleration voltage of 1.5 kV in high vacuum using the secondary electron detection method.

Thickness measurements of membranes were made (50 scans per item, in order to determine the thickness mean value) using a Fischer MP0R magnetic induction coating thickness test instrument.

Density of membranes (ρ) was determined from Archimedes' principle using a top-loading electronic XS105 dual range Mettler Toledo balance provided with a density measurement kit. The samples were sequentially weighed in air and into high purity isooctane at 25 ˚C. Five density measurements were made for each sample. The density was calculated using Eq. (1):

$$\rho = \rho_{liquid}\frac{w_{air}}{w_{air} - w_{liquid}} \quad (1)$$

where ρ_{liquid} is the density of isooctane, w_{air} is the weight of the sample in air, and w_{liquid} is its weight when submerged in isooctane. The theoretical density of the MMMs was determined using Eq. (2):

$$\rho_{MMM} = \frac{1}{\frac{(1-w_f)}{c\rho^{TR} + (1-c)\rho^{PI}} + \frac{w_f}{\rho^f}} \quad (2)$$

where ρ^{PI} and ρ^{TR} are the densities of the neat PI membrane and the neat TR-PBO membrane that were determined from Eq. (1), ρ^f is the density of the filler (0.800 g cm^3) estimated from its skeletal density (1.234 g cm^{-3}) determined by helium pycnometry

(carried out using an Accupyc 1330 device), and its total pore volume (V_f = 0.440 $cm^3\ g^{-1}$) was calculated from low-pressure N_2 isotherms at 77 K. Here, w_f is the weight fraction of the filler in the MMM, and c is the weight fraction of TR-PBO formed during the thermal treatment, which was determined by isothermal TGA analysis from Eq. (3):

$$\text{TR conversion (\%)} = \frac{\text{Experimental loss mass}}{\text{Theoretical loss mass}} \text{x} 100 \quad (3)$$

The fractional free volume (FFV) of membranes was estimated using Eq. (4):

$$FFV = \frac{V_m - 1.3[\,(c\,V_w^{TR} + (1-c)V_w^{PI})(1-\varphi_f) + V_w^f \varphi_f]}{V_m} \quad (4)$$

where V_m is the specific volume of the membrane, V_w^{PI}, V_w^{TR} and V_w^f are the van der Waals volumes of neat polyimide, neat TR-PBO and neat PPN filler, respectively, which were calculated by molecular modeling of the repeat units applying the semiempirical Austin Model (AM1) in the Biovia Materials Studio program.[50] The optimized repeat units were used to determine the molecular volume by constructing a 5-unit polymer structure using the Builder Polymers and Atom Volumes and Surface algorithms. Finally, φ_f is the volume fraction of PPN calculated according to Eq. (5):

$$\varphi_f = \frac{w_f}{w_f + (\frac{\rho^f}{\rho^{PI}})(1-w_f)} \quad (5)$$

Mechanical properties of membranes were evaluated under uniaxial tensile tests at room temperature using an MTS Synergie-200 testing machine equipped with a 100 N load cell. Rectangular test pieces of 5 mm width and 30 mm length were subject to a tensile load applied at 5 mm min^{-1} until fracture.

2.8. Gas permeability measurements

The gas permeability values of the membranes for pure gases (He, O_2, N_2, CH_4 and CO_2) were measured at 30 °C and an upstream pressure of 3 bar using a custom-made constant volume/variable pressure apparatus. Prior to the measurement, the membrane inside the permeation cell was maintained under high vacuum overnight. Then, an upstream pressure of 3 bar was applied (t= 0 s), and the increase in the permeate pressure was recorded as a function of time. All the gases were allowed to permeate until steady-state (ss) conditions were obtained.

The permeability (P) was calculated from Eq. (6):

$$P = \frac{273Vl}{76ATp_o}\left[\left(\frac{dp(t)}{dt}\right)_{ss} - \left(\left(\frac{dp(t)}{dt}\right)_{leak}\right)\right] \quad (6)$$

Here, A is the effective area (cm^2), *l* is the thickness of the membrane (cm), V is the downstream volume (cm^3), T is the absolute temperature (K), p_0 is the upstream pressure

(bar), $(dp(t)/dt)_{ss}$ is the steady state rate of the pressure-rise (mbar s^{-1}), and $(dp(t)/dt)_{leak}$ is the system leak rate (mbar s^{-1}), which was less than 1% of $(dp(t)/dt)_{ss}$.

The ideal selectivity for a pair of gases A and B ($\alpha_{A/B}$) was evaluated as the ratio of the individual gas permeabilities (P_A and P_B), Eq. (7):

$$\alpha_{A/B} = \frac{P_A}{P_B} \quad (7)$$

3. RESULTS AND DISCUSSION

3.1. Synthesis and membrane preparation

The synthesis of precursor polyimides, PIOH and PIOAc, and the protocol for the formation of the corresponding TR-PBOs, TROH and TROAc, were conducted according to our previous reports.[12,16] To examine how PPN filler affects the TR process of polyimides in their corresponding TR-PBOs, MMMs films were made with 15 or 30 wt.% PPN loadings. The chemical structures of the polyimides and PPN are shown in Figure 1. Note that the MMM films were prepared by film casting from PPN-containing a polymer solution. Previous work demonstrated that the use of a low viscosity solvent like THF allowed good dispersions of PPN particles in polyimide solutions, even for high

loadings.[41] The presence of PPN filler in the film was confirmed by the appearance of an IR absorption N-H band at 1470 cm^{-1}, coming from the five-membered lactam rings.

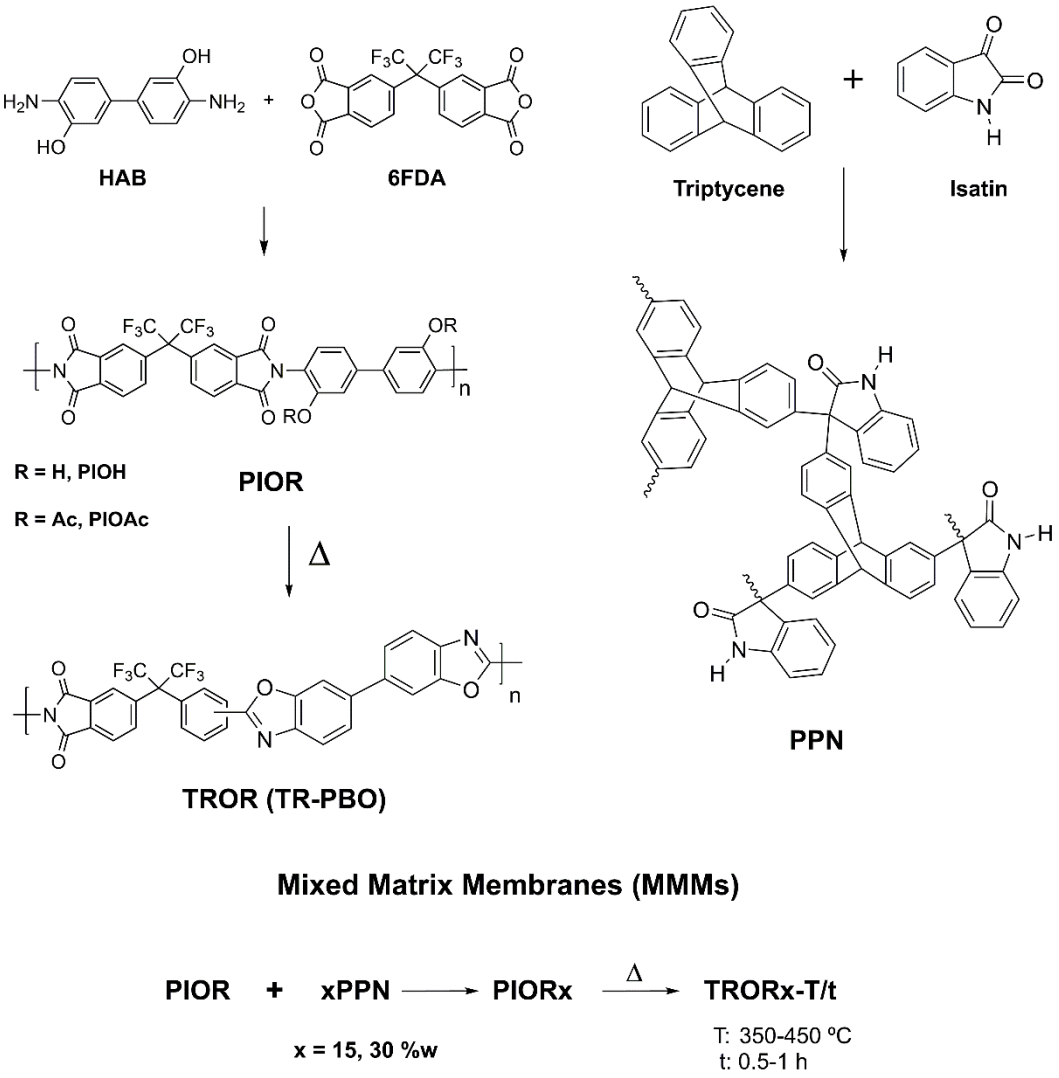

Figure 1. Chemical structures of: (left) PIOH and PIOAc derived from the HAB and 6FDA monomers and TR-PBO formed by thermal treatment, and (right) PPN derived from triptycene and isatin monomers. The bottom scheme indicates how the MMMs were prepared from polyimides and PPN.

3.2. Thermal properties of the filler and membranes

The thermal stability of the polyimide films and of those loaded with PPN particles was studied by dynamic TGA. Thermograms of all neat and composite polyimide films and PPN filler are presented in Figure 2. The PPN-containing films showed two-step weight losses, which are similar to those observed in the neat polyimide films where the first one in the range of the 300-500 °C was associated with the formation of the TR-PBO moiety. This was followed by the second weight loss associated with the thermal degradation of the TR-PBO backbone at around 500-600 °C. The first peaks were broadened toward the high-temperature side with PPN loadings and therefore partially overlapped the degradation peak, indicating that the presence of the filler obviously affected the kinetics of TR-PBO formation.

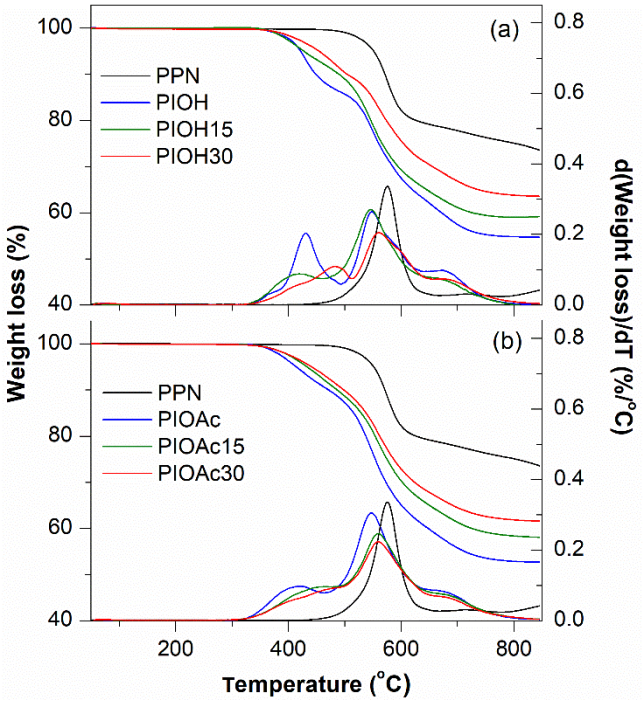

Figure 2. Dynamic TGA curves of (a) PPN, PIOH and (b) PIOAc and the corresponding PPN-containing films.

PPN only showed a single weight loss peak above 500 °C, which was from thermal degradation. The thermal stability of PPN (degradation onset temperature, T_d, ~520 °C) was significantly higher than those of the neat polyimide membranes and MMMs. However, it should be noted that a small degradation of the filler could occur during the preparation of the TR-PBO films.

3.3. Optimization of thermal rearrangement protocol

The conversion protocol of PIOHX and PIOAcX to TR-PBOs was optimized by isothermal TGA analysis. Initially, PIOHX and PIOAcX films were thermally treated

following the protocol previously described by us.[16] This protocol (see Experimental Section) was repeated with the precursor polyimides from another batch for this work to check whether the TR-PBOs were successfully obtained from the similar thermal rearrangement temperature (in the range from 350 to 450 °C) and the isotherm time at that temperature (0.5 and 1 h). It is known that the temperature in a quartz tube furnace can be affected by the variability in the flow rate of gas (pure nitrogen for this work) and thus, the conversion to TR-PBO from precursor polyimide could be variable.

The isotherms obtained from neat polyimide membranes and PPN are shown in the supporting information (SI) section (Figure S1). The weight loss of PIOH and PIOAc films from TR conversion increased when both the rearrangement temperature and the residence time increased. This weight loss of the samples was described as conversion rate, which is the ratio of the experimental weight loss to the theoretical one (14.1% for PIOH and 24.3% for PIOAc) at a particular temperature and residence time. The highest conversion rate of the PIOH film (98 wt.%) to TR-PBO was reached at 450 °C and 30 min. At longer times, the weight loss exceeded the theoretical one, indicating that degradation of TR-PBO took place. The conversion to TR-PBO from the PIOAc film was

64% and 76% at 450 °C for 30 min and 60 min, respectively. All these findings agreed well with those reported earlier.[16]

PPN isotherms revealed the high thermal stability of the material relative to polyimide films. The weight loss did not exceed 3% at 450 °C and 60 min. Although the weight loss could be due to solvent remaining in the pores, a small degradation of the PPN may also occur at temperatures above 400 °C (see Figure 2). The thermal stability of PPN was compared to that of the zeolitic imidazolate framework ZIF-8, which has been widely used as a molecular sieving filler material in MMMs,[37,38,51–56] and to that of Kapton, which is a thermally stable polyimide. For this purpose, isothermal measurements of these samples were carried out at 450 °C for 180 min after subjecting these materials to 300 °C for 60 min. The results are displayed in the Supporting Information section (Figure S2). The isotherms of PPN and ZIF-8 showed a linear weight loss, but the rate of weight loss for ZIF-8 was 6-fold higher than for PPN. In addition, the loss was about 12-fold higher for PPN and 68-fold higher for ZIF-8 relative to Kapton. Thus, it is clear that PPN was sufficiently stable at 450 °C for 30 min and is a suitable filler for use in the preparation of the TR-PBO-based MMMs where high temperature is required.

The thermal formation of the TR-PBO structures in the MMMs was studied by isothermal TGA measurements. Figures 3 (a) and (b) display TGA isotherms of PIOH- and PIOAc-based MMMs, including those of PPN, at 425 °C for 60 min and 450 °C for 30 min. In addition, the theoretical CO_2 weight loss values for each membrane, which were calculated according to the content of PPN, are indicated in the graph. Figures 3(c) and (d) show the conversion degree of polyimide matrix to TR-PBO as a function of the thermal treatment time at those temperatures. To calculate the conversion to TR-PBO, we assumed that the contributions of the polymer matrix and the PPN filler to the overall weight loss of the sample under thermal treatment were additive. Thus, the contribution of the filler to the weight loss isotherm of the MMM was subtracted. This contribution was calculated from the isotherm of pure PPN according to its percentage in the MMM (15 or 30 wt.%). Then, the conversion of the polyimide to TR-PBO of the MMM was determined from Eq. (3), considering the content of polyimide in the membrane.

As expected, the weight loss of MMMs increased over time due to the release of CO_2 during thermal rearrangement process, and the TR conversion increased over time as well. The conversion rate of PIOHX was lower than that of neat PIOH membrane, but the conversion rate was somewhat higher for PIOH30 than for PIOH15. Thus, the addition

of the filler seems to reduce the TR conversion rate of the polyimide matrix from 98% to 92% for PIOH30 and to 89% for PIOH15 when held at 450 °C for 30 min, and from 89% to 78 for PIOH30 and to 71% for PIOH15 when held at 425 °C for 60 min. Regarding PIOAcX, small variations in the conversion values (less than 3%) were observed relative to the pure PIOAc membrane at a particular temperature and residence time.

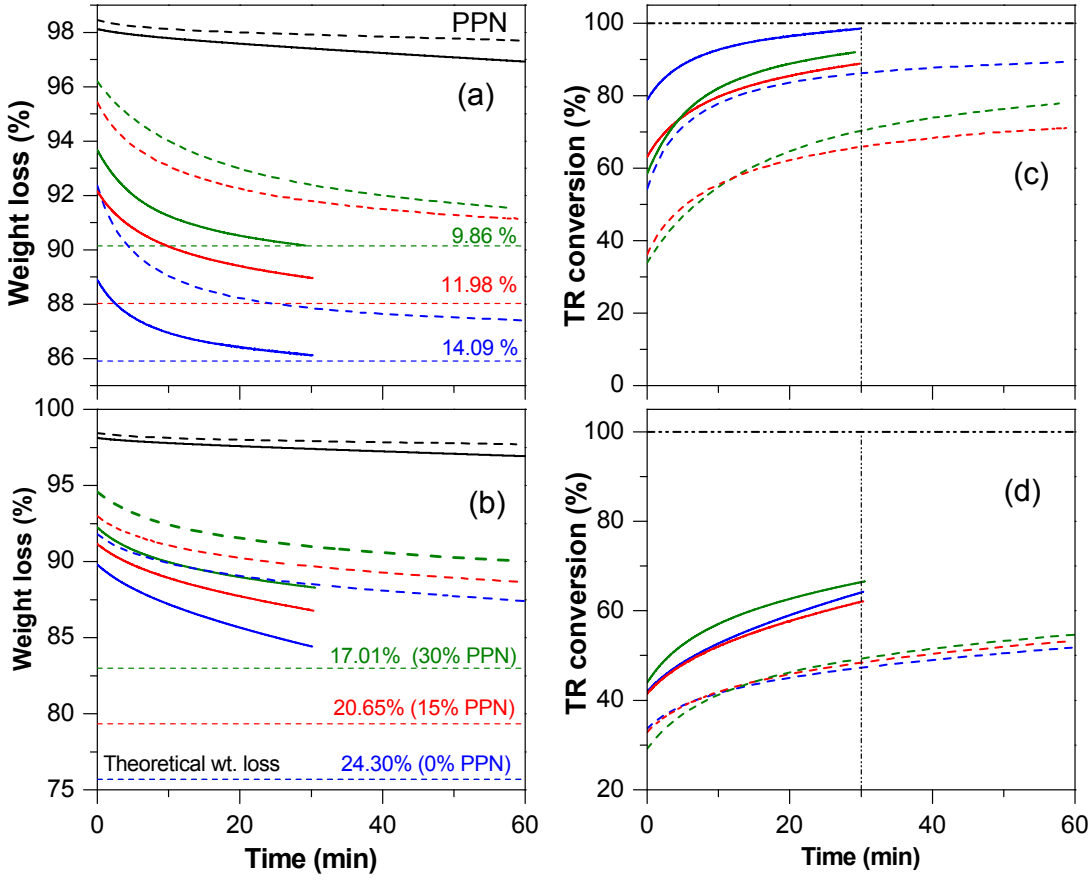

Figure 3. (left) TGA isotherms of neat PPN filler and membranes derived from (a) PIOH and (b) PIOAc, and (right) TR conversion of (c) PIOH- and (d) PIOAc- based membranes as function of thermal treatment: PPN at 425 °C (dashed black line) and 450 °C (solid

black line), neat PIOH and PIOAc at 425 °C (dashed blue lines) and 450 °C (solid blue lines), TROH15-425/60 and TROAc15-425/60 (dashed red lines), TROH15-450/30 and TROAc15-450/30 (solid red lines), TROH30-425/60 and TROAc30-425/60 (dashed green lines), and TROH30-450/30 and TROAc30-450/30 (solid green lines).

To date, there have been few studies on TR-PBO-based MMMs because fillers with very high thermal stability are required. Consequently, the effect of the filler on the TR process is not clear yet.[34,37,57–59] An example of this can be found when nanoparticles of porous and thermostable materials, such as ZIF-8 and PAF-1, were added into TR-able polymers. The incorporation of ZIF-8 nanoparticles accelerated TR conversion in the MMMs. That is, the membranes with higher ZIF-8 content (up to 20 wt.%) required a shorter residence time or lower temperature treatment to achieve the highest conversion (90% at 400 ºC for 60 min)[37] However, the addition of PAF-1 nanoparticles caused the opposite effect in the MMMs. The conversion to TR-PBO was reduced to more than half, i.e., from 52% to 20%, and to 14% at 5 wt.% and 10 wt.% of PAF-1 loading (at 450 °C for 60 min, under continuous evacuation).[34] In a later work, the authors suggested that the interaction of PAF-1 with the TR-precursor polyimide might inhibit the TR conversion reaction. Our results indicate that the addition of PPN did not accelerate the formation of the TR-PBO structure nor inhibit it to the same extent that PAF-1 does.

From all these results, the thermal rearrangement temperature and treatment time for TR-PBO-MMM preparations were chosen on the basis of reaching the highest TR conversion and minimizing the possible degradation of PPN (see Table S2). Thus, the final protocol for obtaining TR-PBO-based MMMs consisted of heating the polyimide-based membranes at 450 °C for 30 min with a heating rate of 5 ^{o}C min^{-1}. From this point on, the TROHX_450/30 and TROAcX_450/30 are referred to as TROHX and TROAcX, where X will continue to be the PPN percentage.

3.4. Chemical structures and physical properties of MMMs

The formation of TR-PBO structure was confirmed by ATR-FTIR analysis. The FTIR spectra of pure polyimide membranes and PPN filler are displayed in Figure S3 (SI section), and the corresponding TR-PBO membranes are shown in Figure S4 (SI section) for comparison. As an example, Figure 4 shows the FTIR spectra of PIOH30, TROH30 and Figure S5 (SI section) those of PIOAc30 and TROAc30. The spectra were normalized to the band that appears at 965 cm^{-1} (C-H bending of aromatic carbons), which did not change in intensity with the thermal treatment, to better compare the differences between them. We observed that the polyimide-based membranes exhibited the typical absorbance bands of polyimide: the stretching vibrations of C=O (1785 and 1715 cm^{-1}), the

asymmetric stretching of C-N (1370 cm^{-1}), and the transverse stretching and the out-of-plane bending of C-N-C (1102 and 720 cm^{-1}). Moreover, the band N-H bending of five-membered lactam rings (1470 cm^{-1}) coming from PPN was visible. The other typical bands of the lactam ring at 1708 and 1320 cm^{-1}, as seen in Figure S3, could not be assigned because their position in the spectrum overlapped with some of the polyimide bands.

After the thermal treatment, the broad hydroxyl band derived from PIOH matrix disappeared and the typical polyimide bands substantially decreased because the conversion to TR-PBO was not complete, as shown by TGA. New bands related to the TR-PBO structure appeared at 1557, 1460 and 1059 cm^{-1}, as seen in Figure S4.[16,17]

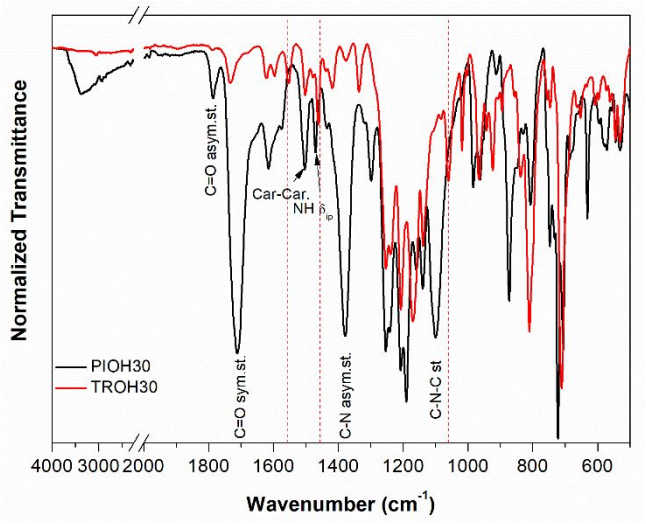

Figure 4. ATR-FTIR spectra of PIOH30 and TROH30. Dashed lines indicate the position of typical bands of TR-PBO moieties.

Wide-angle X-ray scattering (WAXS) measurements revealed the amorphous nature of all the MMMs before and after TR treatment. As an example, Figure 5 compares the WAXS patterns of the PIOH- and TROH-based MMMs, including those of PPN powder

and pristine PI and TR-PBO membranes. All the patterns showed typical broad halos of amorphous polymers with maximum intensities around a 2θ of 15° and a shoulder at the higher scattering angle. It is well-known that the position of the peaks can be related to the most probable intersegmental distance, known as *d*-spacing, between the polymer chains, as calculated from Bragg's equation. Thus, the *d*-spacing could be related to the packing density of the membrane. The addition of the filler caused a peak shift in PI-MMMs towards smaller angle regions from that of neat PI membranes, where higher content of PPN resulted in a higher shift of the maximum. As a result, the maximum shifted from 15.90° (d-spacing of 0.56 nm) for PIOH to 14.90° (0.59 nm) for PIOH30. In addition, the same effect was observed in the patterns of TR-PBO membranes, but the shift was more pronounced. For example, it went from 15.20° (d-spacing of 0.58 nm) for TROH to 13.86° (0.64 nm) for TROH30. These data demonstrate that the presence of PPN particles led to TR-PBO membranes with a lower packing density during TR process, and therefore result in a higher fractional free volume (FFV) for the resulting TR-PBO-MMMs.

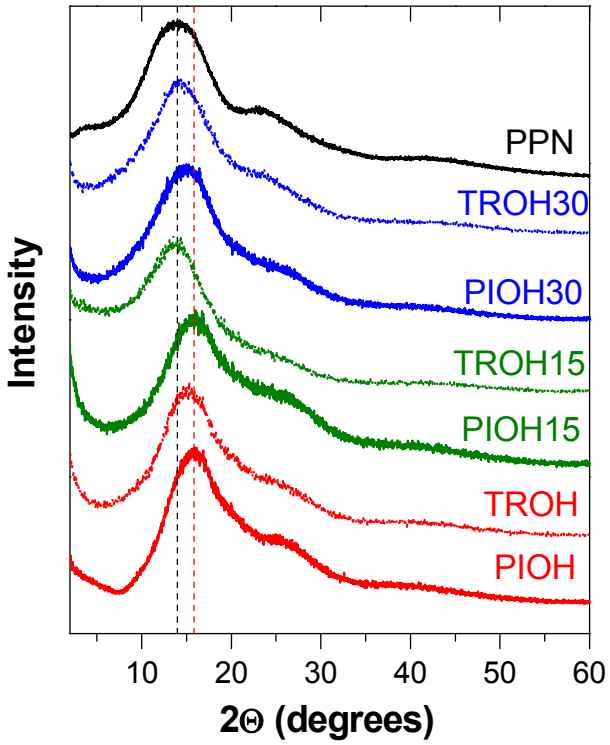

Figure 5. WAXS patterns of PIOH- and TROH- based MMMs, PIOH membrane and PPN powder. The dashed lines indicate the maximum position of PIOH membrane (red) and PPN powder (black).

The experimental and theoretical values of densities and FFVs of the neat polyimide membranes and MMMs were calculated from Eqs. (1), (2) and (4), as listed in Table 1. The experimental densities of the MMMs were lower than those of the neat PI-and neat TR-PBO membranes but were higher than the theoretical densities calculated from Eq. 4. Moreover, several aspects were observed from FFVs of the MMMs: 1) the conversion of PI into TR-PBO caused an increase in the FFV of the neat membranes, which was

consistent with a previous report,[16] 2) the addition of PPN particles increased the FFV of the PI-MMMs (higher content of PPN particles resulted in a higher FFV), and 3) the conversion of PI-MMMs to TR-PBO-MMMs led to a smaller increase in FFV relative to those of neat polyimide membranes. Therefore, it could be stated that the PPN particles prevented efficient chain packing, which was consistent with the observed WAXS results.

Table 1. Densities and fractional free volume of neat membranes and MMMs

Sample	Exp./Theo. Density (g cm^{-3})	FFV	sample	Exp./Theo. density (g cm^{-3})	FFV
PIOH	1.456	0.161	TROH	1.349	0.186
PIOH15	1.367/1.204	0.208	TROH15	1.291/1.162	0.228
PIOH30	1.348/1.059	0.216	TROH30	1.286/1.066	0.233
PIOAc	1.428	0.166	TROAc	1.342	0.196
PIOAc15	1.378/1.189	0.190	TROAc15	1.326/1.166	0.210
PIOAc30	1.357/1.050	0.202	TROAc30	1.304/1.038	0.225

The morphologies of the MMMs were examined using FE-SEM. As an example, the cryogenically-fractured cross-sectional surfaces of the PIOH-and TROH-based MMMs containing 30 wt.% of PPN are shown in Figure 6. The PI-based MMMs exhibited the typical crater-like morphology, which indicates good compatibility between the polymer matrix and the filler. In addition, the small clumps of PPN particles appeared from the

ductile fracture of the membrane. However, after TR treatment, TR-PBO-based membranes showed a smoother surface without any cracks or plastic deformation. In addition, voids around the filler particles (i.e., sieve in a cage effect) were not observed, corresponding with the experimental densities of MMMs that were higher than the theoretical values.

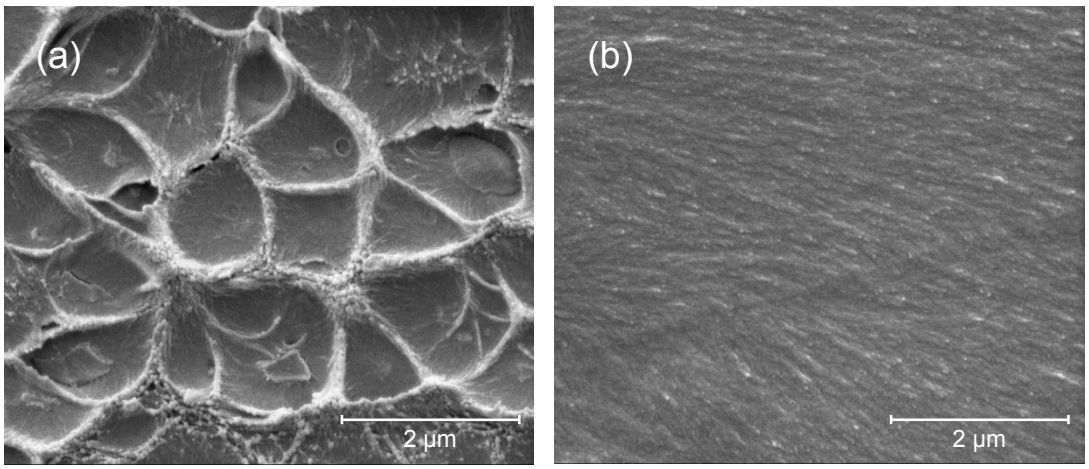

Figure 6. Cross-sectional FE-SEM micrographs of (a) PIOH30 and (b) TROH30.

3.5. Mechanical properties

The mechanical properties of the neat PI and TR-PBO membranes and their PPN containing MMMs are summarized in Table 2. The mechanical strength and ductility of the polyimide membranes decreased after thermal treatment at 450 °C for 30 min. For

example, the TROH membrane showed a decrease of about 9% in the Young's modulus, 30% in the tensile strength, and 60% in the elongation at break relative to PIOH one. The incorporation of PPN particles in the polyimide matrix caused a higher reduction in the Young's modulus of MMMs relative to that of neat polyimide membrane, for instance, a ~30% decrease in a mechanical modulus was observed after incorporating 30 wt.% of PPN content. However, it should be noted that TR-PBO-MMMs retained sufficient mechanical properties to be tested for gas separations applications.

Table 2. Mechanical properties of MMMs and neat PI- and TR-PBO-based membranes

Sample	Young's Modulus (GPa)	Tensile strength (MPa)	Elongation at break (%)
PIOH	2.41 ± 0.04	132 ±9	14 ± 4
PIOH15	1.88 ± 0.02	53 ± 8	6.3 ± 0.2
PIOH30	1.68 ± 0.02	54 ± 9	4.5 ± 0.7
TROH	2.2 ± 0.2	93 ± 1	5.4 ± 0.2
TROH15	1.9 ± 0.2	58 ± 1	3.5 ± 0.1
TROH30	1.9 ± 0.1	61 ± 3	3.4 ± 0.3
PIOAc	2.3 ± 0.2	65 ± 2	4.3 ± 0.5
PIOAc15	2.09 ± 0.08	68 ± 9	3.5 ± 0.5
PIOAc30	1.58 ± 0.07	50 ± 8	2.9 ± 0.6
TROAc	1.95 ± 0.05	74 ± 6	4.3 ± 0.4
TROAc15	1.7 ± 0.1	46 ± 7	3.1 ± 0.5
TROAc30	1.5 ± 0.1	38 ± 5	2.7 ± 0.6

3.6. Gas transport behaviors

Single gas transport properties of the neat PI membranes and PI-MMMs were measured before and after TR treatment with five representative small gases (He, O_2, N_2, CH_4 and CO_2) at 30 °C under 3 bar of pressure difference. The values of gas permeability and ideal selectivity of all the membranes are summarized in Table S3 (SI section). Changes in gas permeability (O_2, N_2, CO_2, and CH_4) and selectivity (O_2/N_2, CO_2/N_2, and CO_2/CH_4) of the MMMs relative to the values of the neat polyimide membranes, PIOH or PIOAc, as a function of the PPN content are graphically displayed in Figure 7. The gas permeability of the PI- and TR-PBO-MMMs increased with the PPN content for all five gases. Moreover, the incorporation of the PPN led to more significant increases in gas permeability for PIOH than PIOAc, for example, CO_2 permeability increased with 2.7 and 4.9-fold for PIOH15 and PIOH30, respectively, relative to PIOH, whereas it improved only about 1.6 and 3.0-fold for PIOAc15 and PIOAc30, respectively, relative to PIOAc. Gas permeability of the PI-MMMs was further enhanced after TR conversion due to the PPN loading. As a result, TROH15, TROH30, TROAc15, and TROAc30 showed 64, 81, 67, 90-fold increases in CO_2 permeability compared to their neat precursors. Note that the neat TROAc exhibited the greatest improvement in gas permeability from TR conversion, which was twice that in the neat TROH for all gases.

This considerable permeability change in TROAc, which was achieved at relatively lower TR conversion (64%), has been induced by the differences in the chain rearrangement mechanisms between PIOH and PIOAc precursors.[16] Furthermore, when TR-PBO-MMMs were compared with their corresponding neat TR-PBOs, the effect of PPN loading on gas permeability was more noticeable in the MMMs derived from TROH. For instance, CO_2 permeability increased 2.6-fold and 3.2-fold for TROH15 and TROH30, but 1.2-fold and 1.7-fold for TROAc15 and TROAc30, respectively.

PIOHX exhibited higher gas selectivity than their TR-PBO derivatives (TROHX), and likewise, neat PI and TR-PBO membranes showed better molecular sieving characteristics than their MMM analogues containing PPN. In fact, the selectivity drop was more significant for the TR process than the addition of PPN particles. Among the PI precursors, PPN particles led to a more significant decrease in gas selectivity for PIOAcX relative to that of PIOHX, especially for the CO_2/N_2 gas pair. Previous results have showed that the use of PPNs in MMMs, which were mainly derived from low-permeability and high-selectivity polyimide matrices, considerably improved their permeability relative to those of the neat polyimide membranes without substantially sacrificing their gas selectivity.[47] Thus, the decrease in selectivity observed in PIOAcX

may be related to a poorer adhesion of the PPN particles to the PIOAc matrix than to the PIOH matrix. After the thermal treatment, the selectivity of TROHX and TROAcX was close to that of the neat TROH and TROAc, indicating that the compatibility between matrix and filler had been improved.

For an in-depth understating of the relationship between polymer-filler compatibility and gas selectivity of MMM, a different type of PIOAcX (PIOAcX_PL) was prepared as a preliminary test using plasma-treated PPN powder, which was previously subjected to a CO_2-plasma treatment for 30 min. It was expected that this CO_2-plasma treatment would incorporate several oxygen-containing functional groups onto the surface of filler, including carboxylic acids, ketones, aldehydes and hydroxyl or epoxy groups, which could improve the adhesion between the PPN and the *ortho*-functional polyimide.[60] Unfortunately, the surface functionalization could not be detected by ATR-FTIR, TGA and CP/MAS 13C NMR spectroscopy due to both the small number of functional groups incorporated and the presence of similar functional groups, carbonyl groups, in the PPN.[41] Significant differences in gas separation properties were found for plasma-treated MMMs derived from PIOAc compared with those without plasma-treatment, but it was not so for those derived from PIOH, which showed similar properties.

The gas permeability and ideal selectivity of PIOAcX_PL before and after thermal treatment are listed in Table S4 (SI section). The results showed an increase in both the permeability and the selectivity of PIOAcX_PL in comparison with those of PIOAcX. For example, CO_2 permeability and CO_2/N_2 selectivity increased by 2.7 and 1.45-fold for PIOAc15_PL and by 2.3 and 1.56-fold for PIOAc30_PL, respectively. The fact that gas selectivity of PIOAcX_PL was closer to that of neat PIOAc membrane could be associated with the better compatibility between the PPN filler and PIOAc matrix in PIOAcX_PL. After thermal treatment, no significant changes in the gas separation properties of TROAcX_PL compared with TROAcX were observed. This finding confirmed that the compatibility between the PPN and PIOAcX matrix improved during the TR-PBO formation regardless of CO_2-plasma treatment on PPN.

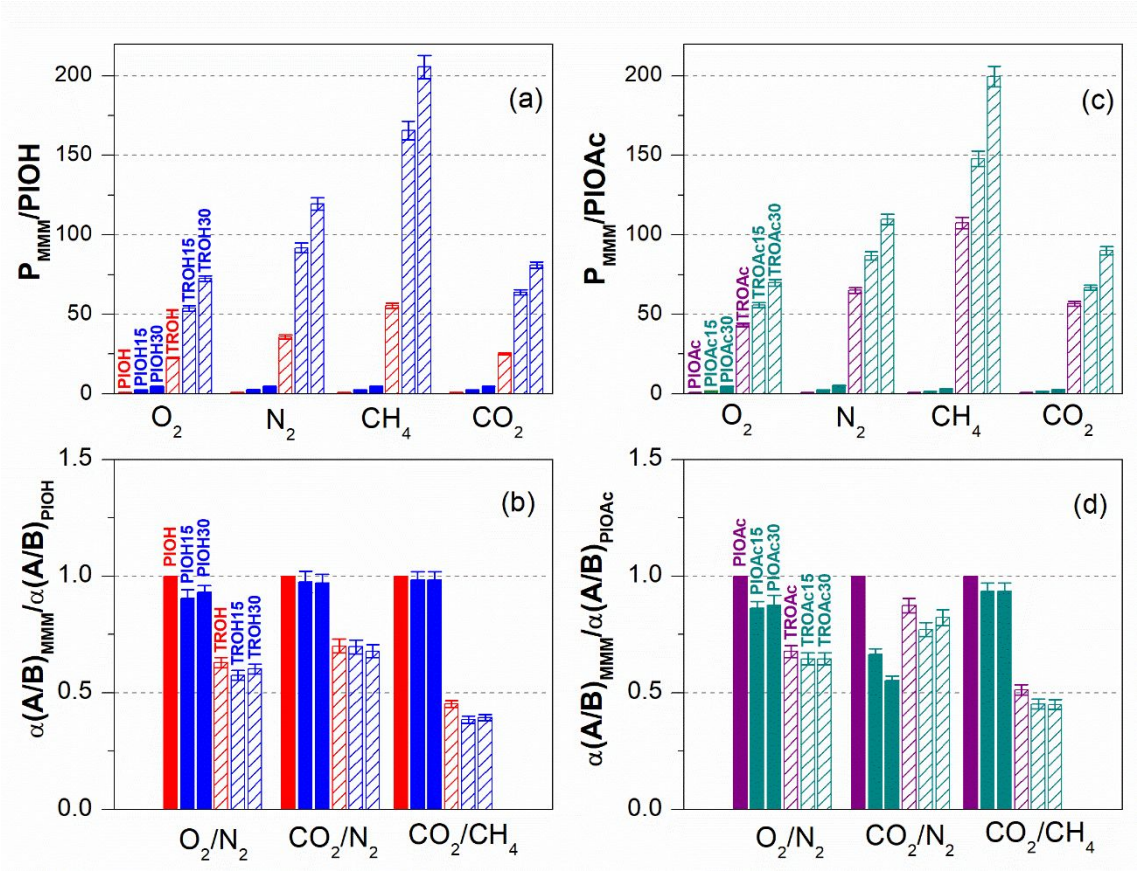

Figure 7. Relative gas permeability (top) and ideal selectivity (bottom) of (a and b) PIOH- and (c and d) PIOAc-based MMMs before and after thermal treatment. The relative values in the graphs were obtained from the normalized permeability (or selectivity) with the corresponding reference polyimide, PIOH or PIOAc.

The gas separation performances of the MMMs were compared to those reported for PPN-based membranes derived from aromatic polyimides, such as Matrimid (low permeability and high selectivity) and 6FDA-TMPD (high permeability and low

selectivity).[47] The results are given on Robeson plots for several gas pairs: CO_2/CH_4 and CO_2/N_2 in Figure 8 and O_2/N_2 in Figure S6 (SI section).[61,62]

The incorporation of PPN particles into polyimide matrices caused a significant improvement in CO_2 gas separation performance of the resulting membranes, which were closer to the 1991 Robeson upper-bound.[61] Even some of these PI-MMMs, such as PIOH30, PIOAc30, and those prepared using the plasma-treated PPN, exceeded the 1991 CO_2/CH_4 upper-bound. Gas separation performance of TR-PBO-MMMs also significantly improved. Particularly, their CO_2/CH_4 separation performance exceeded the 1991 Robeson upper-bound, and even TROAcX slightly surpassed the 2008 upper-bound[62] but the values were far from the new Robeson upper limit for CO_2/CH_4 and CO_2/N_2 separations.[63] Results showed that when a low-permeable polymer matrix (*e.g.,* Matrimid, $P(CO_2)$ ~8.6 Barrer) was used, the gas permeability of the resulting MMMs (*e.g.,* Matrimid with 30 wt.% of PPN, $P(CO_2)$ ~61 Barrer) considerably increased without any reduction in gas selectivity.[47] Similar gas separation behavior was observed in the PI-MMMs derived from PIOAc and PIOH. In contrast, when a high-permeable matrix (*e.g.,* 6FDA-TMPD, $P(CO_2)$ ~444 Barrer) was employed, the increase in gas permeability was relatively smaller (*e.g.,* 6FDA-TMPD with 30 wt.% of PPN, $P(CO_2)$ ~ 710 barrer) with

some loss in gas selectivity. Analogously, TROAcX showed a similar increase in permeability with PPN content, while very small changes in selectivity were observed.

Finally, we should note that the O_2/N_2 separation performance of the TR-PBO-MMMs also showed an evident improvement over the thermally-treated pristine membranes, such that some of the permeability-selectivity values of the membranes exceeded the 1991 Robeson upper bound line, as seen in Figure S6 (SI section).

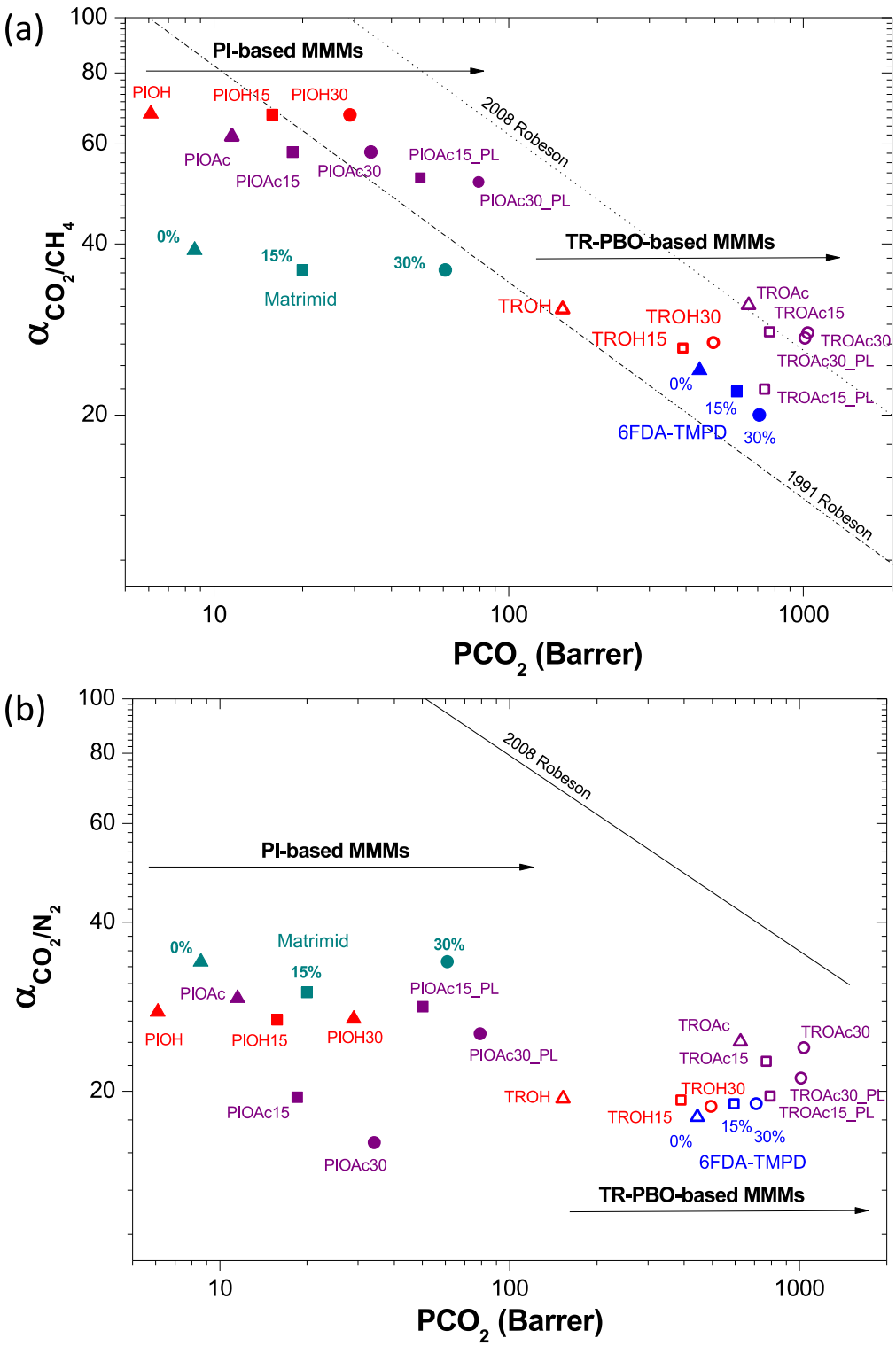

Figure 8. Upper bound limit plot for (a) CO_2/CH_4 and (b) CO_2/N_2 separation by MMMs based on PIOH (solid symbols, red), PIOAc (solid symbols, purple), TROH (empty

symbols, red), TROAc (empty symbols, purple), Matrimid (solid symbols, dark cyan) and 6FDA-TMPD (solid symbols, blue). The filler contents were 0 wt.% (triangle), 15 wt.% (square) and 30 wt.% (circle). The lines correspond to the 1991 and 2008 Robeson upper-bounds.[61,62]

4. CONCLUSIONS

A series of TR-precursor MMMs were prepared by combining aromatic *ortho*-hydroxypolyimide (PIOH) or *ortho*-acetylpolyimide (PIOAc) with different loading (15 and 30 wt%) of a highly microporous network (PPN). SEM images of the MMMs showed relatively good compatibility between the polyimide matrices and the PPN filler, which resulted in the formation of membranes with excellent and homogeneous dispersion of the PPN particles, even for a high loading of 30 wt%.

The thermal resistance of PPN was better than that of the ZIF-8 material that has been widely used as a filler in MMMs and was slightly lower than a very high stable polyimide (such as Kapton) when they were subjected to the thermal treatment used to prepare TR-PBO-MMMs from precursor MMMs. From this finding, TR-PBO-MMMs were successfully prepared without substantial degradation of the loading material.

In general, the polyimide-based MMMs exhibited an increase in gas permeability, due to the presence of PPN, whereas their selectivity values for diverse gas pairs, such as CO_2/N_2 and CO_2/CH_4 were similar. Thus, the high PPN loaded MMMs surpassed the 1991 Robeson limit for CO_2/CH_4. The CO_2 permeability for TROAc30 showed values higher than 1000 Barrer, whereas ideal selectivity was a little bit lower than the pristine TR-PBO materials.

Therefore, microporous high-thermal stable materials were successfully loaded in MMMs, which, after undergoing the thermal rearrangement processes, lead to TR-PBO-MMMs with excellent gas separation properties. In fact, these properties are very competitive for TR materials, and more so when an *ortho*-hydroxypolyimide precursor, with relatively mediocre thermally rearranged gas separation, has been used as polymeric matrix. The results obtained in this work suggest that this filler could be incorporated into other better chosen *ortho*-hydroxypolyimides, presumably generating TR-PBO materials with excellent separations capabilities.

ASSOCIATED CONTENT

Supporting Information

The Supporting Information is available free of charge on the ACS Publications website at DOI.

Key of abbreviations for materials, additional ATR-FTIR spectra and experimental data including TGA and gas transport properties of membranes

AUTHOR INFORMATION

Corresponding Authors

*Yoon Moon Lee- *Department of Energy Engineering, College of Engineering, Hanyang University, 04763 Seoul, Republic of Korea*; orcid.org/0000-0002-5047-3143; *ymlee@hanyang.ac.kr*

*Cristina Álvarez- *Institute of Polymer Science and Technology, ICTP-CSIC, Juan de la Cierva 3, 28006 Madrid, Spain; SMAP UVa-CSIC Research Unit, University of Valladolid, 47071 Valladolid, Spain*; orcid.org/0000-0002-5000-0776; *cristina.alvarez@ictp.csic.es*

Ángel E. Lozano- *Institute of Polymer Science and Technology, ICTP-CSIC, Juan de la Cierva 3, 28006 Madrid, Spain; SMAP UVa-CSIC Research Unit, University of*

Valladolid, 47071 Valladolid, Spain; IU CINQUIMA, University of Valladolid, 47071 Valladolid, Spain; orcid.org/ 0000-0003-4209-3842; *lozano@ictp.csic.es*

Authors

†**Carla Aguilar-Lugo**-*Instituto de Investigaciones en Materiales, Universidad Nacional Autónoma de México, Ciudad Universitaria, Ciudad de Mexico 04510, Mexico;* orcid.org/0000-0003-4700-1564; carla.aguilar@iim.unam.mx

Won Hee Lee- *Department of Energy Engineering, College of Engineering, Hanyang University, 04763 Seoul, Republic of Korea*; orcid.org/0000-0002-9151-8475; wwhhlee@gmail.com

Jesús A. Miguel- *IU CINQUIMA, Universidad de Valladolid, Paseo Belén 5, E-47011 Valladolid, Spain*; orcid.org/0000-0003-2814-5941; jamiguel@uva.es

José G. de la Campa- *Institute of Polymer Science and Technology, ICTP-CSIC, Juan de la Cierva 3, 28006 Madrid, Spain;* orcid.org/0000-0003-1882-3104; jcampa@ictp.csic.es

Pedro Prádanos- *SMAP UVa-CSIC Research Unit, University of Valladolid, 47071 Valladolid, Spain*; orcid.org/0000-0001-8939-8518; ppradanos@uva.es

Joon Yong Bae- *Department of Energy Engineering, College of Engineering, Hanyang University, 04763 Seoul, Republic of Korea*; orcid.org/0000-0002-1890-2630; bjyong0205@hanyang.ac.kr

Author Contributions

The manuscript was written through contributions of all authors. All authors have given approval to the final version of the manuscript.

Carla Aguilar-Lugo: Investigation, Formal analysis, Writing - Original Draft. **Won Hee Lee**: Investigation, Formal analysis, Writing - Review and Editing. **Jesús A. Miguel**: Formal analysis, Data discussion, Funding acquisition. **José G de la Campa**: Formal analysis, data discussion. **Pedro Prádanos**: Formal analysis, data discussion. **Joon Yong Bae**: Investigation. **Young Moo Lee**: Supervision, Funding acquisition, Visualization, Writing - Review and Editing. **Cristina Álvarez**: Conceptualization, Investigation, Supervision, Formal analysis, Writing - Review and Editing. **Ángel E. Lozano**: Conceptualization, Supervision, Formal analysis, Writing - Review and Editing, Funding acquisition.

Funding Sources

This work was supported by Spain's Agencia Estatal de Investigación (AEI) (Projects: PID2019-109403RB-C22 (AEI/FEDER, UE), CTQ2017-89217-P (AEI/FEDER, UE), and PID2019-109403RB-C21 (AEI/FEDER, UE)) and by the Spanish Junta de Castilla y León (VA224P20). This research was partially supported by the Technology Development Program to Solve Climate Change through the National Research Foundation of Korea (NRF) funded by the Ministry of Science and ICT (NRF-2018M1A2A2061979) and by a Korea Institute of Energy Technology Evaluation and Planning (KETEP) grant funded by the Ministry of Trade, Industry & Energy (MOTIE) (20202020800330) of South Korea.

REFERENCES

(1) Du, N.; Park, H. B.; Dal-Cin, M. M.; Guiver, M. D. Advances in High Permeability Polymeric Membrane Materials for CO 2 Separations. *Energy Environ. Sci.* **2012**, *5* (6), 7306–7322. https://doi.org/10.1039/C1EE02668B.

(2) Sanders, D. F.; Smith, Z. P.; Guo, R.; Robeson, L. M.; McGrath, J. E.; Paul, D. R.; Freeman, B. D. Energy-Efficient Polymeric Gas Separation Membranes for a

Sustainable Future: A Review. *Polymer (Guildf).* **2013**, *54* (18), 4729–4761. https://doi.org/10.1016/j.polymer.2013.05.075.

(3) Galizia, M.; Chi, W. S.; Smith, Z. P.; Merkel, T. C.; Baker, R. W.; Freeman, B. D. 50th Anniversary Perspective%: Polymers and Mixed Matrix Membranes for Gas and Vapor Separation: A Review and Prospective Opportunities. *Macromolecules* **2017**, *50* (20), 7809–7843. https://doi.org/10.1021/acs.macromol.7b01718.

(4) Han, S. H.; Kwon, H. J.; Kim, K. Y.; Seong, J. G.; Park, C. H.; Kim, S.; Doherty, C. M.; Thornton, A. W.; Hill, A. J.; Lozano, Á. E.; Berchtold, K. A.; Lee, Y. M. Tuning Microcavities in Thermally Rearranged Polymer Membranes for CO2 Capture. *Phys. Chem. Chem. Phys.* **2012**, *14* (13), 4365. https://doi.org/10.1039/c2cp23729f.

(5) Kim, S.; Lee, Y. M. High Performance Polymer Membranes for CO2 Separation. *Curr. Opin. Chem. Eng.* **2013**, *2*, 238–244. https://doi.org/10.1016/j.coche.2013.03.006.

(6) Pulido, B. A.; Waldron, C.; Zolotukhin, M. G.; Nunes, S. P. Porous Polymeric Membranes with Thermal and Solvent Resistance. *J. Memb. Sci.* **2017**, *539*, 187–196. https://doi.org/10.1016/j.memsci.2017.05.070.

(7) Liang, C. Z.; Chung, T.-S.; Lai, J.-Y. A Review of Polymeric Composite Membranes for Gas Separation and Energy Production. *Prog. Polym. Sci.* **2019**, *97*, 101141. https://doi.org/10.1016/j.progpolymsci.2019.06.001.

(8) Ma, C.; Urban, J. J. Polymers of Intrinsic Microporosity (PIMs) Gas Separation Membranes: A Mini Review. *Proc. Nat. Res. Soc.* **2018**, *2*, 02002. https://doi.org/10.11605/j.pnrs.201802002.

(9) Park, H. B.; Jung, C. H.; Lee, Y. M.; Hill, A. J.; Pas, S. J.; Mudie, S. T.; Van Wagner, E.; Freeman, B. D.; Cookson, D. J. Polymers with Cavities Tuned for Fast Selective Transport of Small Molecules and Ions. *Science (80-.).* **2007**, *318*, 254–258. https://doi.org/10.1126/science.1146744.

(10) Robeson, L. M.; Dose, M. E.; Freeman, B. D.; Paul, D. R. Analysis of the Transport Properties of Thermally Rearranged (TR) Polymers and Polymers of Intrinsic Microporosity (PIM) Relative to Upper Bound Performance. *J. Memb. Sci.* **2017**, *525*, 18–24. https://doi.org/10.1016/j.memsci.2016.11.085.

(11) Liu, Q.; Borjigin, H.; Paul, D. R.; Riffle, J. S.; McGrath, J. E.; Freeman, B. D. Gas Permeation Properties of Thermally Rearranged (TR) Isomers and Their Aromatic

Polyimide Precursors. *J. Memb. Sci.* **2016**, *518*, 88–99. https://doi.org/10.1016/j.memsci.2016.06.026.

(12) Comesaña-Gándara, B.; Calle, M.; Jo, H. J.; Hernández, A.; de la Campa, J. G.; de Abajo, J.; Lozano, A. E.; Lee, Y. M. Thermally Rearranged Polybenzoxazoles Membranes with Biphenyl Moieties: Monomer Isomeric Effect. *J. Memb. Sci.* **2014**, *450*, 369–379. https://doi.org/10.1016/j.memsci.2013.09.010.

(13) Aguilar-Lugo, C.; Álvarez, C.; Lee, Y. M.; de la Campa, J. G.; Lozano, Á. E. Thermally Rearranged Polybenzoxazoles Containing Bulky Adamantyl Groups from Ortho-Substituted Precursor Copolyimides. *Macromolecules* **2018**, *51* (5), 1605–1619. https://doi.org/10.1021/acs.macromol.7b02460.

(14) Lee, W. H.; Seong, J. G.; Hu, X.; Lee, Y. M. Recent Progress in Microporous Polymers from Thermally Rearranged Polymers and Polymers of Intrinsic Microporosity for Membrane Gas Separation: Pushing Performance Limits and Revisiting Trade-off Lines. *J. Polym. Sci.* **2020**, *58* (18), 2450–2466. https://doi.org/10.1002/pol.20200110.

(15) Gleason, K. L.; Smith, Z. P.; Liu, Q.; Paul, D. R.; Freeman, B. D. Pure- and Mixed-Gas Permeation of CO 2 and CH 4 in Thermally Rearranged Polymers Based on

3,3′-Dihydroxy-4,4′-Diamino-Biphenyl (HAB) and 2,2′-Bis-(3,4-Dicarboxyphenyl) Hexafluoropropane Dianhydride (6FDA). *J. Memb. Sci.* **2015**, *475*, 204–214. https://doi.org/10.1016/j.memsci.2014.10.014.

(16) Comesaña-Gándara, B.; De La Campa, J. G.; Hernández, A.; Jo, H. J.; Lee, Y. M.; De Abajo, J.; Lozano, A. E. Gas Separation Membranes Made through Thermal Rearrangement of Ortho-Methoxypolyimides. *RSC Adv.* **2015**, *5*(124), 102261–102276. https://doi.org/10.1039/c5ra19207b.

(17) Calle, M.; Lozano, A. E.; Lee, Y. M. Formation of Thermally Rearranged (TR) Polybenzoxazoles: Effect of Synthesis Routes and Polymer Form. *Eur. Polym. J.* **2012**. https://doi.org/10.1016/j.eurpolymj.2012.04.007.

(18) Lee, W. H.; Bae, J. Y.; Yushkin, A.; Efimov, M.; Jung, J. T.; Volkov, A.; Lee, Y. M. Energy and Time Efficient Infrared (IR) Irradiation Treatment for Preparing Thermally Rearranged (TR) and Carbon Molecular Sieve (CMS) Membranes for Gas Separation. *J. Memb. Sci.* **2020**, *613*, 118477. https://doi.org/10.1016/j.memsci.2020.118477.

(19) Jiang, Y.; Willmore, F. T.; Sanders, D.; Smith, Z. P.; Ribeiro, C. P.; Doherty, C. M.; Thornton, A.; Hill, A. J.; Freeman, B. D.; Sanchez, I. C. Cavity Size, Sorption and Transport Characteristics of Thermally Rearranged (TR) Polymers. *Polymer (Guildf).* **2011**, *52*, 2244–2254. https://doi.org/10.1016/j.polymer.2011.02.035.

(20) Kim, S.; Lee, Y. M. Rigid and Microporous Polymers for Gas Separation Membranes. *Prog. Polym. Sci.* **2015**, *43*, 1–32. https://doi.org/10.1016/j.progpolymsci.2014.10.005.

(21) Lee, W. H.; Seong, J. G.; Bae, J. Y.; Wang, H. H.; Moon, S. J.; Jung, J. T.; Do, Y. S.; Kang, H.; Park, C. H.; Lee, Y. M. Thermally Rearranged Semi-Interpenetrating Polymer Network (TR-SIPN) Membranes for Gas and Olefin/Paraffin Separation. *J. Memb. Sci.* **2021**, *625*, 119157. https://doi.org/10.1016/j.memsci.2021.119157.

(22) Han, S. H.; Misdan, N.; Kim, S.; Doherty, C. M.; Hill, A. J.; Lee, Y. M. Thermally Rearranged (TR) Polybenzoxazole: Effects of Diverse Imidization Routes on Physical Properties and Gas Transport Behaviors. *Macromolecules* **2010**, *43*, 7657–7667. https://doi.org/10.1021/ma101549z.

(23) Liu, Q.; Paul, D. R.; Freeman, B. D. Gas Permeation and Mechanical Properties of Thermally Rearranged (TR) Copolyimides. *Polymer (Guildf).* **2016**, *82*, 378–391. https://doi.org/10.1016/j.polymer.2015.11.051.

(24) Sanders, D. F.; Smith, Z. P.; Ribeiro, C. P.; Guo, R.; McGrath, J. E.; Paul, D. R.; Freeman, B. D. Gas Permeability, Diffusivity, and Free Volume of Thermally Rearranged Polymers Based on 3,3'-Dihydroxy-4,4'-Diamino-Biphenyl (HAB) and 2,2'-Bis-(3,4-Dicarboxyphenyl) Hexafluoropropane Dianhydride (6FDA). *J. Memb. Sci.* **2012**, *409–410*, 232–241. https://doi.org/10.1016/j.memsci.2012.03.060.

(25) Jang, H.; Ha, J.; Yoo, J.; Pyo, J.; Lee, C.; Ryu, T.; Choi, K.; Kim, W. Synthesis and Property of Sulfonated Poly(Methylisatin Biphenylene) Containing Diphenyl Ether by Polyhydroalkylation Reaction. *Int. J. Hydrogen Energy* **2016**, *41* (24), 10466–10472. https://doi.org/10.1016/j.ijhydene.2016.01.050.

(26) Li, S.; Jo, H. J.; Han, S. H.; Park, C. H.; Kim, S.; Budd, P. M.; Lee, Y. M. Mechanically Robust Thermally Rearranged (TR) Polymer Membranes with Spirobisindane for Gas Separation. *J. Memb. Sci.* **2013**, *434*, 137–147. https://doi.org/10.1016/j.memsci.2013.01.011.

(27) Jo, H. J.; Soo, C. Y.; Dong, G.; Do, Y. S.; Wang, H. H.; Lee, M. J.; Quay, J. R.; Murphy, M. K.; Lee, Y. M. Thermally Rearranged Poly(Benzoxazole- Co -Imide) Membranes with Superior Mechanical Strength for Gas Separation Obtained by Tuning Chain Rigidity. *Macromolecules* **2015**, *48*, 2194–2202. https://doi.org/10.1021/acs.macromol.5b00413.

(28) Lee, J.; Kim, J. S.; Moon, S.; Park, C. Y.; Kim, J. F.; Lee, Y. M. Dimensionally-Controlled Densification in Crosslinked Thermally Rearranged (XTR) Hollow Fiber Membranes for CO2 Capture. *J. Memb. Sci.* **2020**, *595*, 117535. https://doi.org/10.1016/j.memsci.2019.117535.

(29) Perez, E.; Karunaweera, C.; Musselman, I.; Balkus, K.; Ferraris, J. Origins and Evolution of Inorganic-Based and MOF-Based Mixed-Matrix Membranes for Gas Separations. *Processes* **2016**, *4*, 32. https://doi.org/10.3390/pr4030032.

(30) Castarlenas, S.; Téllez, C.; Coronas, J. Gas Separation with Mixed Matrix Membranes Obtained from MOF UiO-66-Graphite Oxide Hybrids. *J. Memb. Sci.* **2017**, *526*, 205–211. https://doi.org/10.1016/j.memsci.2016.12.041.

(31) Hsieh, J. O.; Balkus, K. J.; Ferraris, J. P.; Musselman, I. H. MIL-53 Frameworks in Mixed-Matrix Membranes. *Microporous Mesoporous Mater.* **2014**, *196*, 165–174. https://doi.org/10.1016/j.micromeso.2014.05.006.

(32) Jiang, Y.; Liu, C.; Caro, J.; Huang, A. A New UiO-66-NH2 Based Mixed-Matrix Membranes with High CO2/CH4 Separation Performance. *Microporous Mesoporous Mater.* **2019**, *274*, 203–211. https://doi.org/10.1016/j.micromeso.2018.08.003.

(33) Cheng, Y.; Ying, Y.; Zhai, L.; Liu, G.; Dong, J.; Wang, Y.; Christopher, M. P.; Long, S.; Wang, Y.; Zhao, D. Mixed Matrix Membranes Containing MOF@COF Hybrid Fillers for Efficient CO2/CH4 Separation. *J. Memb. Sci.* **2019**, *573*, 97–106. https://doi.org/10.1016/j.memsci.2018.11.060.

(34) Smith, S. J. D.; Hou, R.; Lau, C. H.; Konstas, K.; Kitchin, M.; Dong, G.; Lee, J.; Lee, W. H.; Seong, J. G.; Lee, Y. M.; Hill, M. R. Highly Permeable Thermally Rearranged Mixed Matrix Membranes (TR-MMM). *J. Memb. Sci.* **2019**, *585*, 260–270. https://doi.org/10.1016/j.memsci.2019.05.046.

(35) Lau, C. H.; Konstas, K.; Thornton, A. W.; Liu, A. C. Y.; Mudie, S.; Kennedy, D. F.; Howard, S. C.; Hill, A. J.; Hill, M. R. Gas-Separation Membranes Loaded with Porous

Aromatic Frameworks That Improve with Age. *Angew. Chemie Int. Ed.* **2015**, *54*, 2669–2673. https://doi.org/10.1002/anie.201410684.

(36) Prasetya, N.; Himma, N. F.; Sutrisna, P. D.; Wenten, I. G.; Ladewig, B. P. A Review on Emerging Organic-Containing Microporous Material Membranes for Carbon Capture and Separation. *Chem. Eng. J.* **2020**, *391*, 123575. https://doi.org/10.1016/j.cej.2019.123575.

(37) Kim, J. S.; Moon, S. J.; Wang, H. H.; Kim, S.; Lee, Y. M. Mixed Matrix Membranes with a Thermally Rearranged Polymer and ZIF-8 for Hydrogen Separation. *J. Memb. Sci.* **2019**, *582*, 381–390. https://doi.org/10.1016/j.memsci.2019.04.029.

(38) Japip, S.; Erifin, S.; Chung, T.-S. Reduced Thermal Rearrangement Temperature via Formation of Zeolitic Imidazolate Framework (ZIF)-8-Based Nanocomposites for Hydrogen Purification. *Sep. Purif. Technol.* **2019**, *212*, 965–973. https://doi.org/10.1016/j.seppur.2018.12.016.

(39) Kim, S.; Shamsaei, E.; Lin, X.; Hu, Y.; Simon, G. P.; Seong, J. G.; Kim, J. S.; Lee, W. H.; Lee, Y. M.; Wang, H. The Enhanced Hydrogen Separation Performance of Mixed Matrix Membranes by Incorporation of Two-Dimensional ZIF-L into Polyimide

Containing Hydroxyl Group. *J. Memb. Sci.* **2018**, *549*, 260–266. https://doi.org/10.1016/j.memsci.2017.12.022.

(40) James, J. B.; Lin, Y. S. Thermal Stability of ZIF-8 Membranes for Gas Separations. *J. Memb. Sci.* **2017**, *532*, 9–19. https://doi.org/10.1016/j.memsci.2017.02.017.

(41) Lopez-Iglesias, B.; Suárez-García, F.; Aguilar-Lugo, C.; González Ortega, A.; Bartolomé, C.; Martínez-Ilarduya, J. M.; de la Campa, J. G.; Lozano, Á. E.; Álvarez, C. Microporous Polymer Networks for Carbon Capture Applications. *ACS Appl. Mater. Interfaces* **2018**, *10*, 26195–26205. https://doi.org/10.1021/acsami.8b05854.

(42) Recio, R.; Palacio, L.; Pradanos, P.; Hernandez, A.; Lozano, A. E.; Marcos, A.; de la Campa, J. G.; de Abajo, J. Gas Separation of 6FDA–6FpDA MembranesEffect of the Solvent on Polymer Surfaces and Permselectivity. *J. Memb. Sci.* **2007**, *293*, 22–28. https://doi.org/10.1016/j.memsci.2007.01.022.

(43) Fuhrman, C.; Nutt, M.; Vichtovonga, K.; Coleman, M. R. Effect of Thermal Hysteresis on the Gas Permeation Properties of 6FDA-Based Polyimides. *J. Appl. Polym. Sci.* **2004**, *91*, 1174–1182. https://doi.org/10.1002/app.13189.

(44) Das, M.; Koros, W. J. Performance of 6FDA–6FpDA Polyimide for Propylene/Propane Separations. *J. Memb. Sci.* **2010**, *365*, 399–408. https://doi.org/10.1016/j.memsci.2010.09.029.

(45) Velioğlu, S.; Ahunbay, M. G.; Tantekin-Ersolmaz, S. B. Investigation of CO2-Induced Plasticization in Fluorinated Polyimide Membranes via Molecular Simulation. *J. Memb. Sci.* **2012**, *417–418*, 217–227. https://doi.org/10.1016/j.memsci.2012.06.043.

(46) Velioğlu, S.; Ahunbay, M. G.; Tantekin-Ersolmaz, S. B. Propylene/Propane Plasticization in Polyimide Membranes. *J. Memb. Sci.* **2016**, *501*, 179–190. https://doi.org/10.1016/j.memsci.2015.11.034.

(47) Aguilar-Lugo, C.; Suárez-García, F.; Hernández, A.; Miguel, J. A.; Lozano, Á. E.; de la Campa, J. G.; Álvarez, C. New Materials for Gas Separation Applications: Mixed Matrix Membranes Made from Linear Polyimides and Porous Polymer Networks Having Lactam Groups. *Ind. Eng. Chem. Res.* **2019**, *58*, 9585–9595. https://doi.org/10.1021/acs.iecr.9b01402.

(48) Muñoz, D. M.; Calle, M.; de la Campa, J. G.; de Abajo, J.; Lozano, A. E. An Improved Method for Preparing Very High Molecular Weight Polyimides. *Macromolecules* **2009**, *42*, 5892–5894. https://doi.org/10.1021/ma9005268.

(49) Muñoz, D. M.; de la Campa, J. G.; de Abajo, J.; Lozano, A. E. Experimental and Theoretical Study of an Improved Activated Polycondensation Method for Aromatic Polyimides. *Macromolecules* **2007**, *40*, 8225–8232. https://doi.org/10.1021/ma070842j.

(50) BIOVIA. Dassault Systémes, Biovia Materials Studio, 2017R2, San Diego: Dassault Systèmes, 2017.

(51) Song, Q.; Nataraj, S. K.; Roussenova, M. V.; Tan, J. C.; Hughes, D. J.; Li, W.; Bourgoin, P.; Alam, M. A.; Cheetham, A. K.; Al-Muhtaseb, S. A.; Sivaniah, E. Zeolitic Imidazolate Framework (ZIF-8) Based Polymer Nanocomposite Membranes for Gas Separation. *Energy Environ. Sci.* **2012**, *5*, 8359. https://doi.org/10.1039/c2ee21996d.

(52) Wijenayake, S. N.; Panapitiya, N. P.; Versteeg, S. H.; Nguyen, C. N.; Goel, S.; Balkus, K. J.; Musselman, I. H.; Ferraris, J. P. Surface Cross-Linking of ZIF-8/Polyimide Mixed Matrix Membranes (MMMs) for Gas Separation. *Ind. Eng. Chem. Res.* **2013**, *52*, 6991–7001. https://doi.org/10.1021/ie400149e.

(53) Bushell, A. F.; Attfield, M. P.; Mason, C. R.; Budd, P. M.; Yampolskii, Y.; Starannikova, L.; Rebrov, A.; Bazzarelli, F.; Bernardo, P.; Carolus Jansen, J.; Lanč, M.; Friess, K.; Shantarovich, V.; Gustov, V.; Isaeva, V. Gas Permeation Parameters of Mixed Matrix Membranes Based on the Polymer of Intrinsic Microporosity PIM-1 and the Zeolitic Imidazolate Framework ZIF-8. *J. Memb. Sci.* **2013**, *427*, 48–62. https://doi.org/10.1016/j.memsci.2012.09.035.

(54) Zheng, W.; Ding, R.; Yang, K.; Dai, Y.; Yan, X.; He, G. ZIF-8 Nanoparticles with Tunable Size for Enhanced CO2 Capture of Pebax Based MMMs. *Sep. Purif. Technol.* **2019**, *214*, 111–119. https://doi.org/10.1016/j.seppur.2018.04.010.

(55) Park, S.; Jeong, H.-K. In-Situ Linker Doping as an Effective Means to Tune Zeolitic-Imidazolate Framework-8 (ZIF-8) Fillers in Mixed-Matrix Membranes for Propylene/Propane Separation. *J. Memb. Sci.* **2020**, *596*, 117689. https://doi.org/10.1016/j.memsci.2019.117689.

(56) Carter, D.; Tezel, F. H.; Kruczek, B.; Kalipcilar, H. Investigation and Comparison of Mixed Matrix Membranes Composed of Polyimide Matrimid with ZIF – 8, Silicalite,

and SAPO – 34. *J. Memb. Sci.* **2017**, *544*, 35–46. https://doi.org/10.1016/j.memsci.2017.08.068.

(57) Brunetti, A.; Cersosimo, M.; Kim, J. S.; Dong, G.; Fontananova, E.; Lee, Y. M.; Drioli, E.; Barbieri, G. Thermally Rearranged Mixed Matrix Membranes for CO2 Separation: An Aging Study. *Int. J. Greenh. Gas Control* **2017**, *61*, 16–26. https://doi.org/10.1016/j.ijggc.2017.03.024.

(58) Wang, Y.; Low, Z. X.; Kim, S.; Zhang, H.; Chen, X.; Hou, J.; Seong, J. G.; Lee, Y. M.; Simon, G. P.; Davies, C. H. J.; Wang, H. Functionalized Boron Nitride Nanosheets: A Thermally Rearranged Polymer Nanocomposite Membrane for Hydrogen Separation. *Angew. Chemie - Int. Ed.* **2018**, *57*, 16056–16061. https://doi.org/10.1002/anie.201809126.

(59) Kim, S.; Hou, J.; Wang, Y.; Ou, R.; Simon, G. P.; Seong, J. G.; Lee, Y. M.; Wang, H. Highly Permeable Thermally Rearranged Polymer Composite Membranes with a Graphene Oxide Scaffold for Gas Separation. *J. Mater. Chem. A* **2018**, *6*, 7668–7674. https://doi.org/10.1039/C8TA02256A.

(60) Wavhal, D. S.; Fisher, E. R. Modification of Porous Poly(Ether Sulfone) Membranes by Low-Temperature CO2-Plasma Treatment. *J. Polym. Sci. Part B Polym. Phys.* **2002**, *40*, 2473–2488. https://doi.org/10.1002/polb.10308.

(61) Robeson, L. M. Correlation of Separation Factor versus Permeability for Polymeric Membranes. *J. Memb. Sci.* **1991**, *62*, 165–185. https://doi.org/10.1016/0376-7388(91)80060-J.

(62) Robeson, L. M. The Upper Bound Revisited. *J. Memb. Sci.* **2008**, *320*, 390–400. https://doi.org/10.1016/j.memsci.2008.04.030.

(63) Comesaña-Gándara, B.; Chen, J.; Bezzu, C. G.; Carta, M.; Rose, I.; Ferrari, M.; Esposito, E.; Fuoco, A.; Jansen, J. C.; McKeown, N. B. Redefining the Robeson Upper Bounds for CO2/CH4 and CO2/N2 Separations Using a Series of Ultrapermeable Benzotriptycene-Based Polymers of Intrinsic Microporosity. *Energy Environ. Sci.* **2019**, *12*, 2733–2740. https://doi.org/10.1039/C9EE01384A.

Table of Contents